International Journal of Infrared and Millimeter Waves (2019) 40: 557–573
https://doi.org/10.1007/s10762-019-00584-2

Dielectric Properties of Low-Loss Polymers for mmW and THz Applications

Seckin Sahin[1] · **Niru K. Nahar**[1] · **Kubilay Sertel**[1]

Received: 1 October 2018 / Accepted: 19 March 2019 / Published online: 30 March 2019

Abstract

We present a systematic characterization of dielectric permittivity of 6 commonly used, low-loss polymers namely polystyrene, parylene, polyimide, SLA resin, SU-8, and SUEX for the 100-GHz to 2-THz bands using transmission mode time domain spectroscopy. The dielectric constant and loss tangent for each polymer was systematically recorded using the commercially available TeraView TPS-3000 system and an analytical multilayered media transmission model is used to extract sample permittivity and loss through curve fitting the measured data. Among the studied polymers, polystyrene exhibits the lowest material loss with a loss tangent less than 0.0069 up to 100 GHz to 2 THz. Also, effects of lithographic processing on permittivity and loss for commonly used epoxy-based photoresists SU-8 and SUEX are documented and compared. We show that the dielectric properties of dry film SUEX is comparable with those of SU-8. As such, SUEX is an easy-to-process alternative to commonly used SU-8 for mmW and THz frequency applications.

Keywords Loss tangent · Permittivity · Time domain spectroscopy · SU-8 · SUEX · Parylene · Polyimide · Polystyrene · SLA resin · Terahertz · Millimeter-wave

1 Introduction

To address the spectrum crunch due to the exploding demand for high-rate data connectivity, the millimeter-wave (mmW) band is heavily coveted as a natural expansion

✉ Seckin Sahin
sahin.29@osu.edu

Niru K. Nahar
nahar.2@osu.edu

Kubilay Sertel
sertel.1@osu.edu

[1] Electrical and Computer Engineering, The Ohio State University, Columbus, OH 43212, USA

domain to enable faster access and greater capacity in future wireless networks. Much wider transceiver bandwidths and extremely compact antennas and arrays are the two key technologies that drive the current research in mmW systems, and such high-performance transceiver hardware are becoming commercially available to address the dire need for always-on, high-data-rate connectivity with high spectrum and energy efficiency [1]. In order to realize the industry goal of effectively utilizing the mmW spectrum, novel and cost-effective 5th-generation (5G) transceivers and phased array technologies are in high demand as high-performance wireless nodes in large-scale wireless networks. In particular, thanks to the much smaller wavelengths in the mmW spectrum, the antenna size can be reduced down to a few millimeters, enabling effective system-on-chip solutions with large-scale integration. However, to date a number of key challenges remain to be tackled for on-chip implementation of efficient radiators. Namely, poor bandwidth performance (10–20%) and extremely low radiation efficiencies (5–10%) due to substrate coupling are a key hindrance for on-chip antennas and arrays. Low-loss materials and novel conformal antenna designs that can address substrate coupling issues and improve radiation efficiency are badly needed for fabrication and packaging.

As compared to commonly used semiconductor substrates, thermoplastic polymers, such as polyimide and polystyrene, are relatively easy to process through lamination and exhibit lower material losses. Furthermore, polymer-based photoresists, such as SU-8 and benzocyclobutene (BCB) , have been widely used for RF applications as antenna canopies, radomes, and as common transmission line support materials. Although their dielectric properties are well-studied for RF bands, many polymers have not been studied for mmW and THz band applications. In addition, accurate characterization of inorganic, biological, and fluidic material losses in mmW and THz frequencies is an emerging area of interest [2].

Among available laminates, polystyrene, parylene, polyimide, and SU-8 have been widely utilized for RF and mmW applications. In addition to the above, SUEX is a relatively new, dry film variant of SU-8 which can be externally embossed as a laminate onto semiconductor wafers, allowing for subsequent lithographic processing as thick substrate/superstrate layers for wafer-scale antenna and array realizations [3]. As such, it is an attractive alternative to SU-8 for mmW antenna applications. In addition, materials that are used on commercial additive manufacturing processes are often polymers, such as stereolithographic (SLA) resin, and these have great potential utility in fabrication and packaging of mmW antennas and integrated systems [4].

We note that several of the low-loss polymers presented in this work have been studied previously, as cited throughout the paper. However, considering the sensitivity of measured material characteristics to instrument and environmental variations, a comparative study of the polymers using the same instrument and in a similar environmental setting provides a direct assessment of one material against another. Particularly for low-loss materials used in micro- and nano-fabrication of devices for mmW and THz applications, it is often necessary to conduct such a comparative study prior to developing associated fabrication recipes.

In this paper, we report a systematic characterization of the material properties of the aforementioned polymers using a commercially available THz time-domain spectroscopy system. Particularly, dielectric permittivity and loss tangent of thin

layers of 6 polymers, namely polystyrene, SU-8, SUEX, parylene, polyimide, and SLA resin, were characterized in the 100-GHz–2-THz range using transmission mode spectroscopy. Furthermore, lithographic processing effects (such as UV exposure and curing process) on material losses are also documented for SU-8 and SUEX films. For an accurate model of the material properties, an analytical multilayered media transmission coefficient model is fitted to the measured data through iterative nonlinear least-square method. Using the measured data, we developed a simple polynomial formula that allows for the extrapolation of measured permittivity and loss tangent over a much broader frequency range. The common experimental setup used in the characterization of all polymer samples results in a comprehensive controlled study of the performance of these polymers systematically, as detailed below in Section 2. Section 3 presents the measurement results along with the functional model of permittivity and loss tangent for polystyrene, SU-8, SUEX, parylene, polyimide, and SLA resin where the lithographic processing effects for SU-8 and SUEX are also discussed.

2 Experimental Setup for Permittivity Characterization

The transmission coefficient measurements for the samples studied in this work were performed using a commercial THz time domain spectroscopy (TDS) system (TPS Spectra 3000 from TeraView, Inc). The TDS system allows for real-time measurement of magnitude and phase of the transmission coefficient using the ratio of complex field spectra of the sample and the reference scan without the sample in the device (i.e., a reference measurement in air). In order to prevent artifacts caused by the absorption lines of water vapor and other species in the atmosphere, the measurements were performed in nitrogen-dry environment in the purging chamber of the TDS system. Dielectric properties of polymers can then be extracted from the complex transmission coefficient measurements, as detailed [5]. We note here that only the transmission coefficient can be measured using the TDS system; thus, an analytical extraction of material properties, such as the Nicholson-Ross-Weir (NRW) method [6], cannot be applied using this system. In addition, the measurements were performed over the 60-GHz to 3-THz band; however, only the 100-GHz–2-THz data was used in the analysis due to the low signal-to-noise ratio outside this band. The frequency resolution for the test setup was 3.59 GHz and each frequency data was integrated over 300 measurements to remove random errors from femtosecond mode-locked laser's amplitude fluctuations. The THz-TDS is a coherent system, that is, both the amplitude and phase of a THz signal can be recorded. As such, this coherent detection provides both real and imaginary part of refractive index without resorting to estimations based on Kramers-Kronig relations [7]. Furthermore, the loss tangent and dielectric constant of the materials can be readily obtained from the complex measured refractive index $\epsilon_p = n_p^2$.

To best assess the dielectric permittivity and loss levels, it is most suited to use THz-TDS in transmission mode to get the time domain response of electric field with and without the polymer sample. The analytical model of the transmission through a thin material layer is based on the well-known multilayered media electromagnetic

analysis [8]. We also must note that the root-mean-square (RMS) roughness level of our polymer samples are in the order of few nanometers based on our atomic force microscopy (AFM) measurements. Therefore, we can neglect the associated scattering losses. Considering a transmission through a single dielectric slab, complex transmission coefficient can be written as:

$$\mathcal{T} = \frac{4k_0k_p exp(-jk_p d)}{(k_0 + k_p)^2 - (k_0 - k_p)^2 exp(-2jk_p d)} \tag{1}$$

where k_0 and k_p are the wavenumbers in free space and the thin film, respectively. Here, the film thickness is denoted by d. The above formula assumes a normally incident plane wave and an isotropic homogeneous medium with its complex permittivity related to the complex wavenumber by $k_p = \omega\sqrt{(\mu_0\epsilon_0\epsilon_p)}$. Here, the relative complex permittivity is defined as $\epsilon_p = \epsilon'_p - j\epsilon''_p$. In order to be able to extract a frequency-dependent complex permittivity, we model its real and imaginary parts using second-order polynomials:

$$\epsilon'_p = \theta_1 + \theta_2 f^2 \tag{2}$$

$$\epsilon''_p = \theta_3 + \theta_4 f + \theta_5 f^2 \tag{3}$$

as in [5]. In this analytical model, six unknowns (θ_1, θ_2, θ_3, θ_4, θ_5, d) are determined using an iterative non-linear least-square method to describe the material permittivity and loss over a broad frequency range. We must note that the polynomial model used here does not have a physical meaning. Previously measured data given in [9] and [10] for 200 GHz–4 THz shows that the measurement can be modeled using simple polynomial. By using the polynomial model within the least-square fit, we are eliminating the middle-step of extracting material properties for each frequency in the band of interest and getting a simple representation of material properties, rather than a set of discrete values for each frequency.

Figure 1 illustrates the good agreement between the measured and computed transmission coefficient amplitudes for one of the listed polymers, SLA resin, for completeness. Residual sum of squares for the curve fitting is less than 0.02 for all the measurements.

Material characterization of thin/low index materials requires highly accurate estimation of film thickness, as the multiple reflections of THz signal are not well separated in time domain. In [11–13], the sample thickness and material properties are captured simultaneously using THz-TDS. On the contrary, the polymer samples studies here are thick enough to separate the multiple reflections, thus by keeping the sample thickness as a variable in the curve fitting procedure, accurate characterization of permittivity and loss can be achieved. In all of the polymer samples studies here, the sample thickness determined by least-squares fit was within the ± 3-μm of the measured sample thickness.

3 Measured Dielectric Properties of Thin Film Polymers

Using the approach noted above, we studied 6 different polymers to characterize their dielectric properties. Obviously, none of the samples exhibit magnetic permeability,

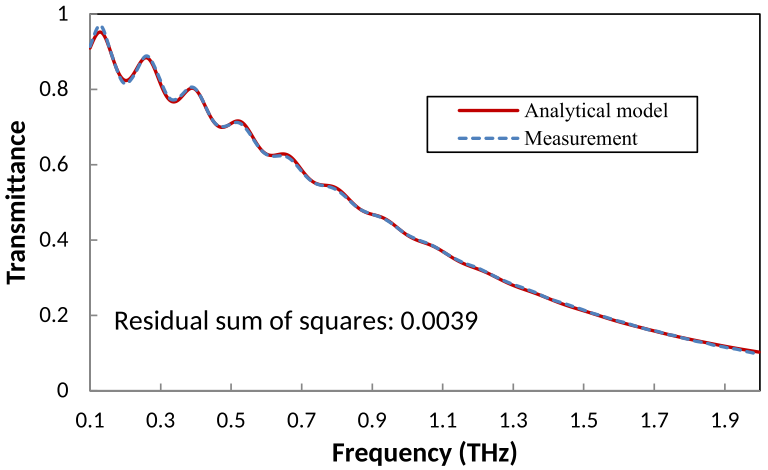

Fig. 1 Measured and computed transmission coefficient amplitudes for SLA resin

so they were assumed to be non-magnetic. Furthermore, for few polymers, we have observed the effects of polymerization on THz transmission properties, leading to a detailed study of dependence of material permittivity on polymerization levels. The results are provided below for each polymer sample.

3.1 SU-8, an Ultra-thick Epoxy-Based Negative Photoresist

IBM first patented SU-8 in 1980s [14], and to date, there have been significant efforts to develop and optimize the SU-8 process as an essential part of microfabrication technology. As described in literature, SU-8 has a thickness range from 1 to 300 μm and few millimeters-thick films can be formed by multiple spin coating [15, 16]. It can be patterned either by UV or X-ray lithography and high-aspect-ratio structures up to 40 can be realized [17]. Furthermore, SU-8 is chemically and mechanically stable [18], and thanks to its low-cost and commonplace availability, cured SU-8 polymer is widely used as a structural material for a wide range of applications.

SU-8 is particularly attractive for mmW and THz applications, where low-loss materials for structural support and packaging are sparse. In particular, it has been studied for wafer-level integration of wideband mmW antennas with RF-front ends for system-on-chip (SoC) applications [3]. There has been a number of studies investigating electrical properties of SU-8 in THz band. Notably, waveguide-based characterization of SU-8 permittivity was reported in [19–21]. However, there has been significant variation in reported values of SU-8 permittivity due to the inaccurate separation of dielectric losses from radiation and conductor losses by 2-port measurement of such devices. In addition, different processing parameters in SU-8 lithography impacts the polymerization levels and consequently their electrical properties.

In our experiments, a carefully monitored cleanroom process is used to produce cross-linked and partially cross-linked SU-8 films. Two 250-μm-thick, 40 mm$\times$40

mm samples were prepared for subsequent characterization and glass wafers were used as substrates. For thick film fabrication, SU-8 2100 from MicroChem Corporation was used. To fabricate the 250-μm-thick SU-8 films, a spin speed of 1500 rpm for 35 s was needed, as specified in material datasheet. Next, the films are soft-baked for 5 min at 65°, followed by 45 min bake at 95°. One of the samples was flood-exposed with 900 mJ/cm^2 dose using UV lithography. Post exposure bake was done for 20 min at 95° and followed by a hard bake for 15 min at 150°. For partially cured SU-8 films, the same recipe was followed with reduced UV exposure dose 300 mJ/cm^2 and without a hard bake step. Then, SU-8 films are released from glass substrates by soaking samples in acetone solution, which provides a rapid temperature change and easy detachment of film from glass substrate.

Immediately following sample preparation, the transmission coefficient was measured using the TDS system and was fitted to the analytical model given in (1) to estimate the polynomial-fit parameters.

As seen in Fig. 2, the extracted real permittivity ϵ'_p varies between 2.73 and 2.54 for fully cured SU-8. However, we observed that the partially cured SU-8 sample exhibits a larger variation in its real permittivity, namely between 3.13 and 2.62. In [22], refractive index for cured SU-8 at 1 THz is roughly about 1.75±0.1, which agrees to our measured results for real permittivity. In [21] and [5], the measured real permittivity for cured SU-8 is above 3.2 for 30 GHz and 200 GHz, respectively. These previous papers reported slightly larger permittivity values than our results; however, such differences can be attributed to variations in sample processing parameters in SU-8 lithography.

The loss tangent of SU-8 is also given in Fig. 2 where the fully cross-linked SU-8 exhibits a loss tangent $tan\delta$ of 0.019 and 0.058 at 100 GHz and 2 THz, respectively. Measured $tan\delta$ for partially cross-linked SU-8 was 0.059 and 0.081 at 100 GHz and 2 THz, respectively. The measurement results show that the partially cross-linked sample exhibits larger losses than the fully cross-linked SU-8. Therefore, full polymerization is recommended to reduce dielectric losses for mmW and THz bands.The measured loss tangent values in previous studies [20] and [21] are 0.02 ± 0.001 for W-band (75–110 GHz) and 0.027 at 30 GHz, respectively. These results are in an

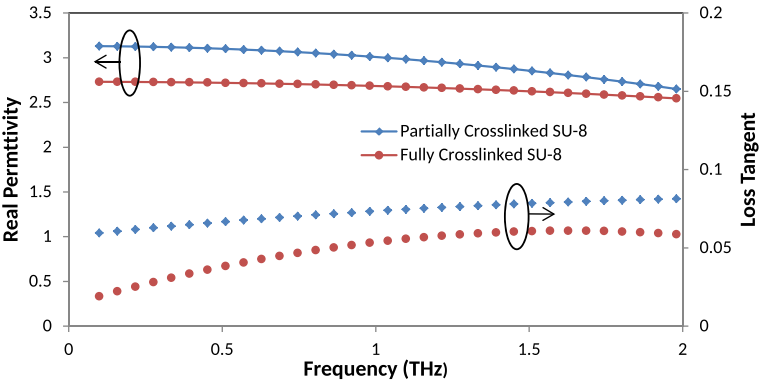

Fig. 2 Measured real permittivity and loss tangent as a function of frequency for two SU-8 samples

agreement with our findings. In [5], the loss tangent is measured as 0.027 at 200 GHz and 0.055 at 1 THz, which agrees very well with our results.

3.2 SUEX, Epoxy-Based Dry Film Resist

SUEX films are commercially available from DJ MicroLaminates in varying thicknesses and shapes. Development and optimization of its fabrication process has been investigated in several studies [23, 24] and potential applications include plating molds for metal microstructures, structural polymer in MEMS, wafer-level packaging applications, flexible circuits etc. We have previously studied the material properties of SUEX [25] and it proved to be a viable alternative to SU-8 as a structural component for mmW and THz applications.

Since lithography using commercially available liquid resists is often quite complicated and time-consuming, dry thick films are developed to overcome those manufacturing difficulties. SUEX is a thick epoxy resist sheet that can be manufactured with different shapes and thicknesses from 100 μm to few millimeters. Lamination of these films to different substrates takes only minutes, which offers significant utility compared to other materials commonly used in microelectromechanical systems (MEMS) fabrication. SUEX shows better transparency than other epoxy films, making it more preferable for thick resist applications [26]. Excellent uniformity, resolution, and high quality of sidewalls are key attributes of SUEX dry films [26]. Much like SU-8, SUEX can also be patterned using either UV or X-ray lithography or hot imprinting/embossing the surface. Furthermore, SUEX can also be processed as free-standing microstructures or be laminated to the different substrates [26].

A 1-in. diameter, 150-μm-thick UV-cured (cross-linked) and green (pre-cross-linked) samples were provided by DJ MicroLaminates.

Figure 3 shows the measured data for the real part of SUEX permittivity from 100 GHz to 2 THz. The effect of polymerization can again be clearly noticed in the measured data. Green SUEX films exhibit higher real and imaginary permittivity and

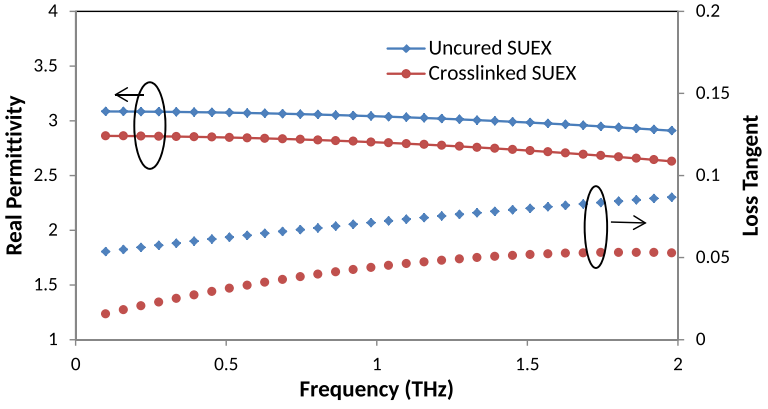

Fig. 3 Measured permittivity and loss tangent of two SUEX samples as a function of frequency

thus higher material losses. Extracted real permittivity for green SUEX film ranged from 3.08 at 100 GHz to 2.91 at 2 THz. For cross-linked SUEX film, real permittivity reduces from 2.86 to 2.62, at 100 GHz and 2 THz, respectively.

The loss tangents for the green and cross-linked SUEX samples are shown in Fig. 3. As seen, the measured loss tangent for the cross-linked SUEX film is 0.015 and 0.052 at 100 GHz and 2 THz, respectively. For green SUEX film, loss tangent was measured to be 0.051 at 100 GHz and 0.087 at and 1 THz. These results indicate that green SUEX films exhibits 82% more material loss than fully cross-linked SUEX.

When we compare partially cross-linked SU-8 and uncured SUEX, real permittivity results are consistent with each other. For uncured samples, SU-8 has 2.7% higher real permittivity than SUEX. Measured loss tangent values for green samples are in an agreement as well. Uncured SU-8 film is 4% lossier than green SUEX film. For cured samples, SUEX has 4% higher real permittivity than SU-8 and it exhibits 16% less material loss than the corresponding SU-8 film. As material properties of SU-8 highly depend on the processing parameters such as curing temperatures, resting time, UV exposure, it is expected to see slight differences in material properties of SU-8 and SUEX films. Nevertheless, the material characterization approach presented here provides consistent results showing that SUEX films exhibit lower material losses than SU-8.

3.3 Polyimide

Polymers play a crucial role as dielectric layers in current state-of-the-art microelectronics technology [27]. They can be used as packaging material for integrated circuit (IC) chips, and also as intermetallic dielectric layers. Furthermore, they can be utilized as photoresist in lithography steps in microfabrication. Polyimide is a commonly used material due to combination of superior properties such as its ability to withstand extreme temperature, vibration, and other challenging environments, it finds diverse applications in aerospace, defense, automotive, and industrial applications [28]. Specifically, polyimide has been used as a substrate in THz metamaterial applications [29], as a part of high-performance nanocomposites [30, 31], and in liquid crystal alignments [28].Polyimide can also be used as an interlayer dielectric material in high-intensity interconnections, thanks to having thermal stability and high planarization capabilities [27]. As such, several studies promote polyimide as an integral part of interconnect systems [32, 33].

Here, we utilized two different polyimide films; a 125-μm-thick Kapton® HN general purpose polyimide film sample was provided by DuPont™and another 200-μm-thick polyimide film (Cirlex) was provided from Fralock. The DuPont™polyimide is rated for $-269°$ to 400°, and furthermore, it can be laminated, metallized or adhesive coated [34].

Figure 4 exhibits the real permittivity as a function of frequency. Extracted real permittivity for Kapton film varies from 3.43 at 100 GHz to 3.27 at 2 THz. For Cirlex film, extracted values are 3.46 at 100 GHz and 3.34 at 2 THz.

Overall, measurement results for two polyimide films were quite consistent with each other. Furthermore, we note that the above measurements for polyimide are also in good agreement with the results reported in [35, 36]. In [35], polyimide

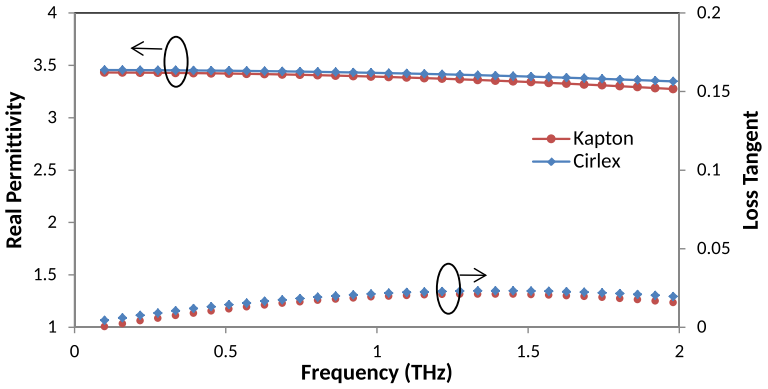

Fig. 4 Real permittivity and loss tangent as a function of frequency for Kapton and Cirlex polyimides

dielectric constant is measured as 3.45 at 1 THz, which fits perfectly well with our measurement results.

3.4 Polystyrene

Polystyrene is one of the most well-known of polymers, and exhibits low loss in the THz regime. It has been used in lens designs [37], and also to minimize the reflection losses in lens-air interface [9, 38]. Previous studies have focused on different forms of polystyrene. In [39], three polystyrene foams with different mass densities were characterized by the THz-TDS system, as they can be used as dichroic filters, which block near IR and transmit THz radiations [39]. Another group [9] investigated THz properties of cross-linked polystyrene (PSX), a well-known far-infrared polymer, which has different thermal and mechanical properties than normal polystyrene. To study the permittivity and loss of polystyrene in mmW and THz bands, we used a 220-μm-thick, 40mm$\times$40mm-wide sample for characterization.

Also plotted in Fig. 5 is the real part of polystyrene permittivity which is around 2.6 and stable throughout 100-GHz–2-THz frequency range. As shown in Fig. 5, the measured loss tangent is almost constant around 0.006.

Our measured data is in a good agreement with previous studies [9, 10, 40]. Real permittivity is measured as 2.55 for 200-GHz–4-THz bands in [9], which matches well with our measurements. Moreover, in [10], the measured real permittivity is 2.56 along 100-GHz–1-THz range. We must note that the result from [7] contradicts with the rest of the reported literature.

Overall, real and imaginary permittivity of polystyrene is low and nearly constant throughout 100 GHz-2 THz band. Also it exhibits very low material losses, again making it ideal for THz applications.

3.5 Parylene-N

Parylene is a common name for a polymer that has 20 variants [41]. Parylene-N is one of most commonly used member of the Parylene family along with Parylene-C

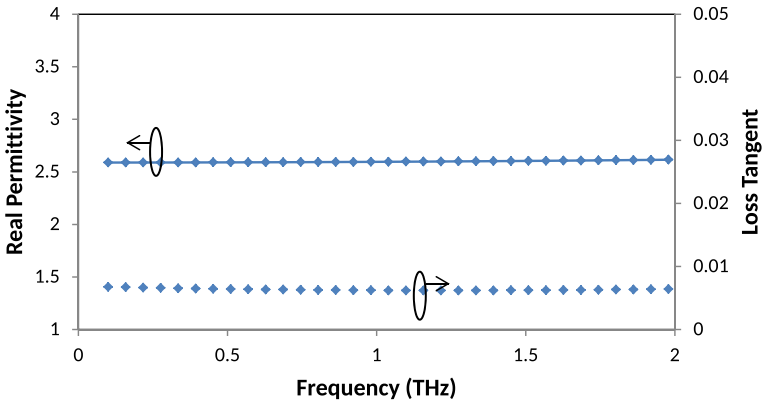

Fig. 5 Permittivity and loss tangent results for polystyrene film

and Parylene-D. Thanks to its superior mechanical and electrical properties, Parylene has found wide range of applications in many areas of nanotechnology, electronics and medical devices [41]. Apart from its applications in MEMS and wafer-level packaging, Parylene is a very popular anti-reflection (AR) coating material in THz frequencies [42, 43]. This polymer can be deposited on various substrates by chemical vapor deposition (CVD). Parylene coating by CVD process achieves superior quality of conformal coating compared to liquid coating techniques, as gaseous monomers can uniformly coat sharp corners, edges and cavities [41]. Coatings made from parylene are conformal and pinhole free on any substrate [44]. Also, Parylene films can be relieved from the substrate after deposition. In addition, Parylene is an excellent thermoplastic with thermal stability, good adhesion properties, chemical inertness and low water absorption [42]. Moreover, Parylene exhibits low loss and has a low dielectric constant. Coupled with its ability to form high-quality defect-free thin films makes Parylene very attractive for THz applications. Also being compatible with human biology, it may even find applications in biomedical applications using THz waves.

In our experiment, we used a 6-μm Parylene-N coating on a glass slide, obtained from Para Tech Coating [44]. The thin Parylene film was peeled from the glass slide for the material characterization. Due to the extremely thin Parylene-N sample, very small changes in the transmission signal were observed, leading to increased uncertainty in characterization.

Despite the concerns related to film thickness, there is still a good match between measurement and analytical results, especially for the high-frequency end. In Fig. 6, we illustrate the permittivity results for Parylene-N. Parylene-N permittivity was measured to be approximately 2.6 and almost constant across the measurement band. As shown in Fig. 6, the loss tangent is approximately 0.058. Previous works [42, 43] and the datasheet [44] show consistent results with our characterization. As another example, in [42], the real permittivity is given around 2.6 for THz band. Furthermore, another study [41] for Parylene-C gives higher permittivity and higher loss

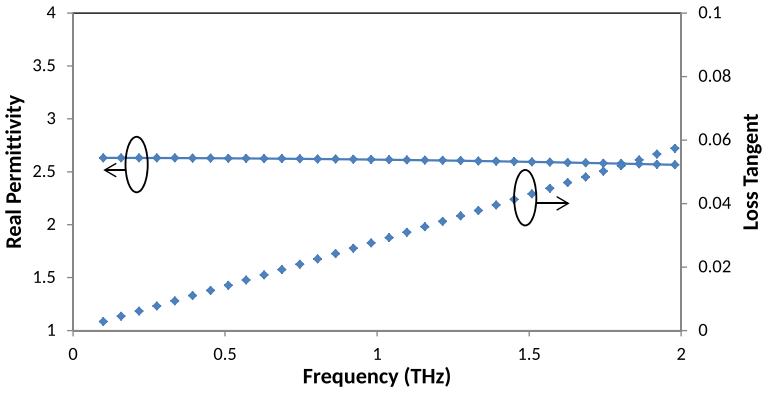

Fig. 6 Permittivity and loss tangent results of Parylene-N as a function of frequency

tangent compared to our measurements for Parylene-N, which is consistent with the datasheet.

3.6 SLA Resin

Stereolithography (SLA) is an automated additive fabrication method where a liquid photopolymer resin is patterned by a focused UV laser or a LED light source through photopolymerization [4]. This technique was first patented in 1986 [45], and implementation of process improvements leads to a SLA with a far better resolution, to nano-metric scales [46]. By using SLA, 3D objects can be printed directly from computer-aided drawings, without any alignment, bonding or any other intermediate steps. It is a rapid prototyping technology and plays an important role in commercialization of polymeric microdevices. Specifically, it can be considered as a new manufacturing method for mmW and THz passive components such as waveguides, horn antennas, mirrors [47]. Here, we note that microstructures printed by SLA can be coated with metal as a second step for completion of passive components [47]. Previous studies [48–51] show the potential use of SLA printing for mmW and THz device fabrication.

There are number of SLA printers commercially available along with compatible photopolymer resins. A wide variety of photopolymer materials is available for different applications which may require high-temperature resistance, flexibility, and durability. Although mechanical and thermal properties for each resin are widely reported in the company datasheets [52], electrical properties have typically not been studied before. SLA-based printers could potentially be used to prototype devices that can be used for high-frequency applications; thus, accurate characterization of their electrical properties is necessary. In our study, we used Formlabs Form 2 SLA 3D printer and photopolymer resin Tough FLTOTL04. We printed a 680-μm-thick sample for material characterization.

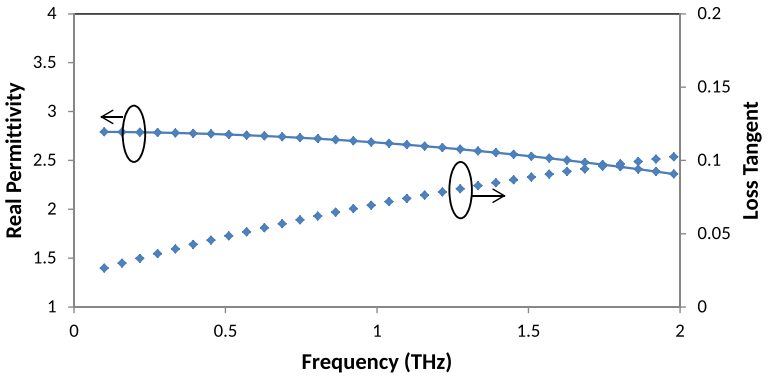

Fig. 7 Measured permittivity and loss tangent results for SLA film as a function of frequency

The permittivity of SLA resin ranges from 2.8 at 100 GHZ down to 2.35 at 2 THz. The measured loss tangent given in Fig. 7 is around 0.021 at 100 GHz and increases up to 0.103 at 2 GHz.

Next, we summarize the characterization results of the 6 polymers studied above.

4 Results and Discussion

The polymers characterized above are suitable base materials for high-frequency applications. Although they are all commercially available with reported material properties, they had not previously been well characterized in the mmW and THz bands. Here, we presented a systematic study of the dielectric properties of SU-8 and SUEX, polyimide, polystyrene, SLA resin, and Parylene in 100-GHz–2-THz range. Also, we have extrapolated our model to get the material properties for lower frequencies.

Table 1 summarizes the real permittivity values of 6 polymers at 100 GHz, 200 GHz, 1 THz, and 2 THz. Measured loss tangent values at those frequencies are

Table 1 Measured real permittivity results

Material	ϵ'_p (0.2 THz)	ϵ'_p (1 THz)	ϵ'_p (2 THz)
SU-8	$2.73 \pm 4.1\%$	$2.68 \pm 4.2\%$	$2.54 \pm 4.9\%$
SUEX	$2.86 \pm 1.2\%$	$2.80 \pm 1\%$	$2.62 \pm 1\%$
Kapton polyimide	$3.43 \pm 2.1\%$	$3.39 \pm 2.2\%$	$3.27 \pm 2.9\%$
Cirlex polyimide	$3.45 \pm 1.8\%$	$3.43 \pm 1.8\%$	$3.34 \pm 1.8\%$
Polystyrene	$2.59 \pm 0.85\%$	$2.59 \pm 0.9\%$	$2.62 \pm 1.2\%$
SLA Resin	$2.79 \pm 0.5\%$	$2.68 \pm 1.1\%$	$2.35 \pm 2.2\%$
Parylene-N	2.63	2.61	2.56

Table 2 Measured loss tangent results

Material	$tan\delta$ (0.2 THz)	$tan\delta$ (1 THz)	$tan\delta$ (2 THz)
SU-8	$0.0250 \pm 13.8\%$	$0.0540 \pm 4.5\%$	$0.0580 \pm 2.36\%$
SUEX	$0.0200 \pm 9.9\%$	$0.0440 \pm 3.1\%$	$0.0520 \pm 2.4\%$
Kapton polyimide	$0.0035 \pm 70\%$	$0.0194 \pm 27\%$	$0.0153 \pm 10.2\%$
Cirlex polyimide	$0.0071 \pm 34\%$	$0.0213 \pm 15\%$	$0.0192 \pm 10\%$
Polystyrene	$0.0067 \pm 60\%$	$0.0062 \pm 22\%$	$0.0064 \pm 16\%$
SLA Resin	$0.0310 \pm 2.25\%$	$0.0700 \pm 0.407\%$	$0.1030 \pm 1.87\%$
Parylene-N	0.0056	0.0280	0.0580

given in Table 2. We have only included cured, fully-cross-linked SU-8 and SUEX properties for a reasonable comparison. Uncertainty in the permittivity and loss tangent is examined by applying the least-squares fit to the set of 10 samples over the same frequency range. The variations in the calculated permittivity and loss tangents are also given in Tables 1 and 2.

Among these 6 polymers, polystyrene exhibits the lowest material loss for high-frequency applications. Furthermore, it is low-cost and widely available in many forms such as transparent or opaque films or foams with different mass densities.

On the other hand, the epoxy-based polymers SU-8 and SUEX have similar chemical formulations; therefore they also exhibit similar material properties. However slight differences are expected as there are various factors affecting the material properties of SU-8 such as processing time and temperature, level of polymerization, impurities, and solvent content [5, 53]. Overall, cured SUEX has slightly higher dielectric constant and less material losses compared to SU-8, which is a popular and well-studied material in MEMS and in microfabrication as a permanent photoresist. Thus, it may be advantageous to use SU-8 in a conventional cleanroom facility. Alternatively, SUEX is a dry film and can be applied to any substrate with a simple office laminator. Although SUEX is quite new to the industry, it eliminates the long and sensitive processing steps needed for liquid epoxy-based resists.

Polyimide has the highest dielectric constant, yet fairly low-loss performance among the studied materials. Polyimide is a preferred material for many applications as being commercially available with different thermal and physical properties. Furthermore, it is thermally and mechanically stable with desirable electrical properties, which makes it an ideal interlayer dielectric material. It can be laminated to the various substrates and metals or stand alone as a flexible substrate for high-frequency applications. After all, it is a well-studied material as SU-8 and has several variants for different applications.

As 3D printing became ubiquitous for rapid prototyping, stereolithographic resins continue to find applications in new devices and systems. However, as characterized above and as expected, SLA Resins exhibit relatively higher losses among the other materials studied here. Nonetheless, it exhibits key advantages as it replaces typical lithographic processing steps with a 3D printer. This could significantly accelerate

the design and prototyping process and further UV curing of SLA samples could result in lower material losses.

Along with polystyrene, Parylene-N exhibits the lowest loss for THz applications. High-quality conformal Parylene-N depositions can be performed via CVD techniques, however, it is more expensive than the other polymers studied here. Also, Parylene-N also has a limited thickness range due to the CVD fabrication.

5 Conclusion

We reported a systematic study of permittivity and loss performance of 6 polymers using THz time domain spectroscopy system. Particularly, dielectric permittivity and loss tangent of SU-8, SUEX, polyimide, polystyrene, SLA resin, and Parylene in 100-GHz– 2-THz range was presented. For a consistent study, an analytical multi-layered transmission model was fitted to the measured data using iterative non-linear least square method. Among the characterized polymers, polystyrene is preferable as having the lowest dielectric constant and loss tangent. In addition, SU-8 and SUEX have close permittivity results as having similar formulations [54] and both materials are ideal structural components with high resolution microfabrication. Polyimide has higher dielectric constant compared to other polymers, but may find applications as a low-loss flexible substrate and as a structural material in high-frequency devices. SLA resin has the highest material losses, while being the most practical material for rapid prototyping. Finally, Parylene-N has the best loss performance after polystyrene and it can be utilized as the lens coating material or high-quality thin film substrates for THz applications. In short, those polymers are the strong candidates of future mmW and THz devices due to their preferable loss performance and microfabrication capabilities advantages, and here, we documented a systematic and comparative study of their electrical properties to help foster their utility.

Acknowledgments This work is supported in part by Office of Naval Research Program No: N00014-14-1-0810 and National Science Foundation under Grant No. ECCS-1444026 and CNS-1618566. Any opinions, findings, and conclusions or recommendations expressed in this material are those of the author(s) and do not necessarily reflect the views of the Office of Naval Research or the National Science Foundation.

References

1. J. Thompson, X. Ge, H.-C. Wu, R. Irmer, H. Jiang, G. Fettweis, and S. Alamouti, "5G wireless communication systems: prospects and challenges [guest editorial]," *IEEE Communications Magazine*, vol. 52, no. 2, pp. 62–64, 2014.
2. S. Liu, N. D. Orloff, C. A. Little, W. Zhao, J. C. Booth, D. F. Williams, I. Ocket, D. M.-P. Schreurs, and B. Nauwelaers, "Hybrid characterization of nanolitre dielectric fluids in a single microfluidic channel up to 110 ghz," *IEEE Transactions on Microwave Theory and Techniques*, 2017.
3. S. Sahin, N. K. Nahar, and K. Sertel, "On-chip UWB phased arrays for mmW connectivity," *2016 IEEE International Symposium on Antennas and Propagation (APSURSI)*, pp. 1495–1496, 2016.
4. A. K. Au, W. Lee, and A. Folch, "Mail-order microfluidics: evaluation of stereolithography for the production of microfluidic devices," *Lab on a Chip*, vol. 14, no. 7, pp. 1294–1301, 2014.

5. N. Ghalichechian and K. Sertel, "Permittivity and loss characterization of SU-8 films for mmW and Terahertz applications," *IEEE Antennas and Wireless Propagation Letters*, vol. 14, pp. 723–726, 2015.
6. E. J. Rothwell, J. L. Frasch, S. M. Ellison, P. Chahal, and R. O. Ouedraogo, "Analysis of the Nicolson-Ross-Weir method for characterizing the electromagnetic properties of engineered materials," *Progress In Electromagnetics Research*, vol. 157, pp. 31–47, 2016.
7. Y.-S. Jin, G.-J. Kim, and S.-G. Jeon, "Terahertz dielectric properties of polymers," *Journal of the Korean Physical Society*, vol. 49, no. 2, pp. 513–517, 2006.
8. W. C. Chew, *Waves and fields in inhomogeneous media*. IEEE New York, 1995.
9. A. Podzorov and G. Gallot, "Low-loss polymers for Terahertz applications," *Applied Optics*, vol. 47, no. 18, pp. 3254–3257, 2008.
10. R. Piesiewicz, C. Jansen, S. Wietzke, D. Mittleman, M. Koch, and T. Kürner, "Properties of building and plastic materials in the THz range," *International Journal of Infrared and Millimeter Waves*, vol. 28, no. 5, pp. 363–371, 2007.
11. I. Pupeza, R. Wilk, and M. Koch, "Highly accurate optical material parameter determination with THz time-domain spectroscopy," *Optics express*, vol. 15, no. 7, pp. 4335–4350, 2007.
12. L. Duvillaret, F. Garet, and J.-L. Coutaz, "A reliable method for extraction of material parameters in terahertz time-domain spectroscopy," *IEEE Journal of selected topics in quantum electronics*, vol. 2, no. 3, pp. 739–746, 1996.
13. T. D. Dorney, R. G. Baraniuk, and D. M. Mittleman, "Material parameter estimation with terahertz time-domain spectroscopy," *JOSA A*, vol. 18, no. 7, pp. 1562–1571, 2001.
14. V. C. Pinto, P. J. Sousa, V. F. Cardoso, and G. Minas, "Optimized SU-8 processing for low-cost microstructures fabrication without cleanroom facilities," *Micromachines*, vol. 5, no. 3, pp. 738–755, 2014.
15. H. Lorenz, M. Despont, N. Fahrni, J. Brugger, P. Vettiger, and P. Renaud, "High-aspect-ratio, ultra-thick, negative-tone near-UV photoresist and its applications for MEMS," *Sensors and Actuators A: Physical*, vol. 64, no. 1, pp. 33–39, 1998.
16. E. H. Conradie and D. F. Moore, "SU-8 thick photoresist processing as a functional material for MEMS applications," *Journal of Micromechanics and Microengineering*, vol. 12, no. 4, p. 368, 2002.
17. J. D. Williams and W. Wang, "Study on the postbaking process and the effects on UV lithography of high aspect ratio SU-8 microstructures," *Journal of Micro/Nanolithography, MEMS, and MOEMS*, vol. 3, no. 4, pp. 563–568, 2004.
18. MicroChem, "SU-8, negative tone photoresist formulations 50-100," 2002. Technical Data Sheet.
19. J. M. Dewdney and J. Wang, "Characterization the microwave properties of SU-8 based on microstrip ring resonator," *Wireless and Microwave Technology Conference*, pp. 1–5, 2009.
20. C. Collins, R. Miles, R. Pollard, D. Steenson, J. Digby, G. Parkhurst, J. Chamberlain, N. Cronin, S. Davies, and J. W. Bowen, "Millimeter-wave measurements of the complex dielectric constant of an advanced thick film UV photoresist," *Journal of Electronic Materials*, vol. 27, no. 6, pp. L40–L42, 1998.
21. F. D. Mbairi and H. Hesselbom, "High frequency design and characterization of SU-8 based conductor backed coplanar waveguide transmission lines," *International Symposium on Advanced Packaging Materials: Processes, Properties and Interfaces*, pp. 243–248, 2005.
22. M. Naftaly and R. E. Miles, "Terahertz time-domain spectroscopy for material characterization," *Proceedings of the IEEE*, vol. 95, no. 8, pp. 1658–1665, 2007.
23. D. W. Johnson, J. Goettert, V. Singh, and D. Yemane, "SUEX process optimization for ultra-thick high-aspect ratio LIGA imaging," *Proc. SPIE*, p. 79722U, 2011.
24. K. Mateti, R. A. Byrne-Dugan, C. D. Rahn, and S. A. Tadigadapa, "Monolithic SUEX flapping wing mechanisms for pico air vehicle applications," *Journal of Microelectromechanical Systems*, vol. 22, no. 3, pp. 527–535, 2013.
25. S. Sahin, N. K. Nahar, and K. Sertel, "Permittivity and loss characterization of SUEX epoxy films for mmW and THz applications," *IEEE Transactions on Terahertz Science and Technology*, vol. 8, no. 4, pp. 1–6, 2018.
26. D. Johnson, A. Voigt, G. Ahrens, and W. Dai, "Thick epoxy resist sheets for MEMS manufacturing and packaging," *IEEE International Conference on Micro Electro Mechanical Systems (MEMS)*, pp. 412–415, 2010.
27. A. Kuntman and H. Kuntman, "A study on dielectric properties of a new polyimide film suitable for interlayer dielectric material in microelectronics applications," *Microelectronics Journal*, vol. 31, no. 8, pp. 629–634, 2000.

28. D.-J. Liaw, K.-L. Wang, Y.-C. Huang, K.-R. Lee, J.-Y. Lai, and C.-S. Ha, "Advanced polyimide materials: syntheses, physical properties and applications," *Progress in Polymer Science*, vol. 37, no. 7, pp. 907–974, 2012.
29. H. Tao, A. Strikwerda, K. Fan, C. Bingham, W. Padilla, X. Zhang, and R. Averitt, "Terahertz metamaterials on free-standing highly-flexible polyimide substrates," *Journal of Applied Physics*, vol. 41, no. 23, p. 232004, 2008.
30. C.-M. Leu, Y.-T. Chang, and K.-H. Wei, "Polyimide-side-chain tethered polyhedral oligomeric silsesquioxane nanocomposites for low-dielectric film applications," *Chemistry of Materials*, vol. 15, no. 19, pp. 3721–3727, 2003.
31. T. Tanaka, G. Montanari, and R. Mulhaupt, "Polymer nanocomposites as dielectrics and electrical insulation-perspectives for processing technologies, material characterization and future applications," *IEEE transactions on Dielectrics and Electrical Insulation*, vol. 11, no. 5, pp. 763–784, 2004.
32. P. Rickerl, J. Stephanie, and P. Slota, "Processing of photosensitive polyimides for packaging applications," *IEEE Transactions on Components, Hybrids, and Manufacturing Technology*, vol. 10, no. 4, pp. 690–694, 1987.
33. G. Samuelson, "Polyimide for multilevel very large-scale integration (VLSI)," ACS Publications, 1982.
34. DuPont, "Kapton summary of properties," 2011. Technical Data Sheet.
35. P. D. Cunningham, N. N. Valdes, F. A. Vallejo, L. M. Hayden, B. Polishak, X.-H. Zhou, J. Luo, A. K.-Y. Jen, J. C. Williams, and R. J. Twieg, "Broadband Terahertz characterization of the refractive index and absorption of some important polymeric and organic electro-optic materials," *Journal of Applied Physics*, vol. 109, no. 4, pp. 043505–043505, 2011.
36. M. Walther, A. Ortner, H. Meier, U. Löffelmann, P. J. Smith, and J. G. Korvink, "Terahertz metamaterials fabricated by inkjet printing," *Applied Physics Letters*, vol. 95, no. 25, p. 251107, 2009.
37. S. Busch, M. Weidenbach, M. Fey, F. Schäfer, T. Probst, and M. Koch, "Optical properties of 3D printable plastics in the THz regime and their application for 3D printed THz optics," *Journal of Infrared, Millimeter, and Terahertz Waves*, vol. 35, no. 12, pp. 993–997, 2014.
38. C. E. Zah and D. B. Rutledge, "A polystyrene cap for matching a silicon lens at Millimeter wavelengths," *International Journal of Infrared and Millimeter Waves*, vol. 6, no. 9, pp. 909–917, 1985.
39. G. Zhao, M. Ter Mors, T. Wenckebach, and P. C. Planken, "Terahertz dielectric properties of polystyrene foam," *Journal of Optical Society of America*, vol. 19, no. 6, pp. 1476–1479, 2002.
40. J. Birch, "The far-infrared optical constants of polypropylene, PTFE and polystyrene," *Infrared physics*, vol. 33, no. 1, pp. 33–38, 1992.
41. X. Liu, S. MacNaughton, D. B. Shrekenhamer, H. Tao, S. Selvarasah, A. Totachawattana, R. D. Averitt, M. R. Dokmeci, S. Sonkusale, and W. J. Padilla, "Metamaterials on parylene thin film substrates: Design, fabrication, and characterization at Terahertz frequency," *Applied Physics Letters*, vol. 96, no. 1, p. 011906, 2010.
42. A. Gatesman, J. Waldman, M. Ji, C. Musante, and S. Yagvesson, "An anti-reflection coating for silicon optics at Terahertz frequencies," *IEEE Microwave and Guided Wave Letters*, vol. 10, no. 7, pp. 264–266, 2000.
43. H.-W. Hübers, J. Schubert, A. Krabbe, M. Birk, G. Wagner, A. Semenov, G. Goltsman, B. Voronov, and E. Gershenzon, "Parylene anti-reflection coating of a quasi-optical hot-electron-bolometric mixer at Terahertz frequencies," *Infrared Physics & Technology*, vol. 42, no. 1, pp. 41–47, 2001.
44. P. T. C. Inc, "Parylene properties," 2010. Technical Data Sheet.
45. C. W. Hull, "Apparatus for production of three-dimensional objects by stereolithography," Mar. 11 1986. US Patent 4,575,330.
46. A. Bertsch and P. Renaud, "Microstereolithography," in *Three-Dimensional Microfabrication Using Two-photon Polymerization*, pp. 20–44, Elsevier, 2016.
47. A. Macor, E. De Rijk, S. Alberti, T. Goodman, and J.-P. Ansermet, "Note: Three-dimensional stereolithography for millimeter wave and terahertz applications," *Review of Scientific Instruments*, vol. 83, no. 4, p. 046103, 2012.
48. D. Wu, N. Fang, C. Sun, X. Zhang, W. J. Padilla, D. N. Basov, D. R. Smith, and S. Schultz, "Terahertz plasmonic high pass filter," *Applied Physics Letters*, vol. 83, no. 1, pp. 201–203, 2003.
49. A. von Bieren, E. De Rijk, J.-P. Ansermet, and A. Macor, "Monolithic metal-coated plastic components for Mm-wave applications," *IEEE International Conference on Infrared, Millimeter, and Terahertz waves*, pp. 1–2, 2014.

50. S. Kirihara, M. Kaneko, and T. Niki, "Terahertz wave control using ceramic photonic crystals with a diamond structure including plane defects fabricated by microstereolithography," *International Journal of Applied Ceramic Technology*, vol. 6, no. 1, pp. 41–44, 2009.
51. M. D'Auria, W. J. Otter, J. Hazell, B. T. Gillatt, C. Long-Collins, N. M. Ridler, and S. Lucyszyn, "3-D printed metal-pipe rectangular waveguides," *IEEE Transactions on Components, Packaging and Manufacturing Technology*, vol. 5, no. 9, pp. 1339–1349, 2015.
52. Formlabs, "Tough photopolymer resin," 2017. Technical Data Sheet.
53. O. P. Parida and N. Bhat, "Characterization of optical properties of SU-8 and fabrication of optical components," *International Conference on Optics and Photonics*, pp. 4–7, 2009.
54. DJMicroLaminates, "SUEX epoxy thick film sheets (TDFS)," 2017. Preliminary Data Sheet.